

Evidence for parallel confinement in resonant charge transfer of H^- near metal surfaces

Himadri S. Chakraborty, Thomas Niederhausen, and Uwe Thumm

*James R. Macdonald Laboratory, Department of Physics,
Kansas State University, Manhattan, Kansas 66506-2604, USA*

(Dated: November 5, 2018)

Using a wave packet propagation approach, we find that the resonant charge transfer process of H^- near a Cu(111) surface is strongly influenced by transient hybrid states. These states originate from an ion-induced confinement parallel to the surface together with the surface-localization character of the metal potential along the surface normal. The lowest members of these states have lifetimes of the order of interaction times in typical particle-surface scattering experiments. The propagation of the electron probability density provides clear evidence for this effect in visualizing the evolution and the decay of these transient states.

PACS numbers: 79.20.Rf, 34.70.+e, 73.20.At

The investigation of electron transfer and orbital hybridization processes during the interaction of a projectile atom or ion with a metal surface is of both fundamental and practical importance. The ensuing knowledge finds valuable use in various applied fields of physics, such as, development of ion sources, control of ion-wall interactions in fusion plasma, surface chemistry and analysis, secondary ion mass spectroscopy, and reactive ion etching[1, 2]. Of basic interest is the detailed understanding of single-electron transfer leading to either ionization or neutralization of a surface-scattered projectile. This process of resonant charge transfer (RCT) has been addressed by employing different non-perturbative theoretical methods, including single-center basis-set-expansion[3], complex coordinates rotation[4], two-center expansion[5], multi-center expansion techniques[6], and the direct numerical integration of the effective single-electron Schrödinger equation by Crank-Nicholson wave packet propagation (CNP)[7, 8, 9, 10].

Of all these methods, CNP is most flexible in the sense that it can readily be applied to any parametrized effective potential that may be used to represent the electronic structure of substrate and projectile. In contrast to expansion methods that usually simplify the target to a free-electron (jellium) metal, CNP allows for a significantly more detailed representation of the substrate electronic structure, including the effect of band gaps[7, 11], surface states[8], and image states on the RCT dynamics.

The Cu(111) surface is of particular interest since (a) the affinity level of H^- lies within the L -band gap of the surface and (b) it serves as a prototype of a metal surface that can localize a surface state within its band gap. We show that for the H^- /Cu(111) system charge transfer is to a large extent channeled through transient hybrid states that are confined parallel to the surface by the combined influence of surface and projectile potentials. H^- is described by an effective potential that models the interaction of the active electron with a polarizable core[12]. A one-dimensional [in the co-ordinate (z) of surface normal] single-electron effective potential,

constructed from pseudopotential local density calculations, is employed to model the surface[13]. This potential reproduces the observed and/or *ab initio* L -band gap position, surface state and image states for zero electron momentum component k_{par} parallel to the surface (x direction). Note that the first image state lies in the band gap while higher ones are degenerate with the conduction band[13]. We employ the CNP[9, 10] of the initial free H^- wave function ϕ_{ion} over a two-dimensional numerical grid in which the metal continuum is approximated by free electronic motion in x direction. Our grid includes 100 layers on the bulk and extends to $z = 200$ a.u. on the vacuum side. The topmost layer of lattice points defines $z = 0$. The grid covers 200 a.u. in x . The grid spacings $\Delta z = \Delta x = 0.2$ a.u. yield good convergence.

For fixed ion-surface distances D , the numerical propagation over time t yields $\Phi(t)$ and the ionic survival amplitude $A(t) = \langle \Phi(t) | \phi_{\text{ion}} \rangle$. The real part of the Fourier transform (FT) of this amplitude yields the projected density of states (PDOS) that exhibits resonance structures. The position, width, and amplitude of these resonances provide, respectively, the energy, lifetime, and population of the states. Contrary to the parametric fitting adopted in Ref. 8, a direct FT of $A(t)$ is performed by propagating, in time-steps $\Delta t = 0.1$ a.u., over a period long enough for acceptable convergence. Figure 1 depicts the PDOS (thick solid curve) for three typical values of D . Results neglecting the electronic motion parallel to the surface are obtained by propagating over a one-dimensional grid along z and are shown (short-dashed curve) for comparisons. Note, although for this 1-D propagation, due to the absence of any decay continuum, $A(t)$ never fully converges, we still carry out the FT of $A(t)$ calculated over a finite time, since we are interested only in identifying resonances in the 1-D PDOS.

At $D = 11$ a.u. [Fig 1(a)], our results with or without the parallel motion included show discretized structures corresponding to the valence and conduction band. The affinity level resonance (at -1.56 eV) and the surface state resonance (at -5.31 eV) are also present in both cal-

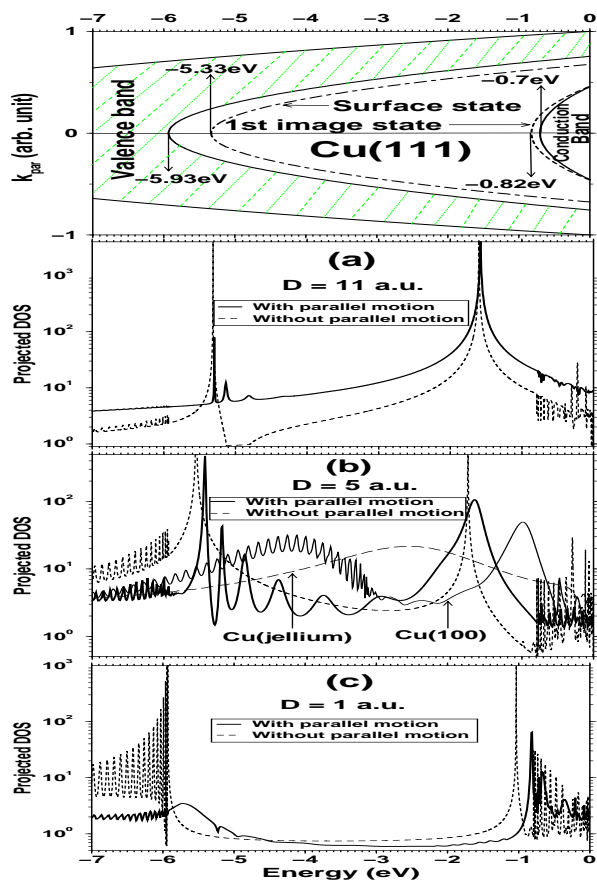


FIG. 1: Top panel: Schematic of the Cu(111) band structure as a function of k_{par} showing a surface state at -5.33 eV within the gap separating the valence and the conduction band; (a) PDOS for $D = 11$ a.u. for Cu(111); (b) $D = 5$ a.u. for Cu(111), Cu(100), and Cu-jellium; (c) $D = 1$ a.u. for Cu(111).

culations, although the affinity level is shifted downward from the unperturbed asymptotic affinity of -0.76 eV. Strikingly, two small peaks appear just above the surface state resonance for the results that include the parallel motion. For $D = 5$ a.u. [Fig. 1(b)], the affinity level and the surface state resonance are present in both results, with and without parallel motion, *but* the structures in between for the calculation that incorporates electronic parallel motion increase in number and strength. Clearly, these new resonances appear only when the electronic parallel degree of freedom is switched on. For a jellium Cu surface the PDOS [Fig. 1(b), long-dashed curve] only shows a wide affinity level peak, as expected, thus indicating that the resonances are due to details in the surface band structure that are not accounted for in the simplistic jellium model. For a more complete portrayal of the origin of these features we also show the PDOS [Fig. 1(b), thin solid curve], including the parallel motion, for Cu(100), which has a similar band gap in the direction normal to the surface but, contrary to Cu(111), *no* surface state inside the gap[13]. This shows valence band structures up to -3.1 eV and the affinity level at -1 eV

but no significant feature in between. Evidently, the extra features in the Cu(111) PDOS between the surface state and the affinity level resonances *must* be originating both from the parallel degree of freedom of the electron and the special localizing property of the Cu(111) potential along the surface normal that binds a surface state inside the band gap. For very close ion-surface separation, $D = 1$ a.u., these features almost disappear, while two similar resonances superimposed on the conduction band spearhead, at -0.67 and -0.35 eV [Fig. 1(c)], above the affinity level. These resonances, in analogy with the ones below the affinity level, also originate from the electron parallel motion and the weak binding of the long-range tail of the surface potential.

The origin and evolution of this effect with decreasing D can be understood as follows. As H^- moves towards the surface, the ion potential gradually deepens following, at large D , the classical image interaction. Consequently, the spherical symmetry of the ion potential gets broken by the surface potential “slope”, which becomes steepest in the vicinity of metal-vacuum interface. Sufficiently close to the surface, the parallelly-stretched asymmetric top of the ion potential confines a new state. Although this state is bound in the parallel direction, whether or not it will live long will depend on how much binding it experiences in the direction normal to the surface. Indeed, for Cu(111) the surface potential has enough reflectivity to enable the formation of a localized surface state within the band gap. As a consequence, the new state, confined parallelly by the incoming ion, is also (temporarily) bound in the normal direction by the Cu(111) potential. This state is relatively long-lived and appears as a fairly narrow peak in the PDOS spectrum [Fig 1(a)]. As the ion moves closer to the surface, the number of states confined parallelly increases and additional peaks emerge in the PDOS [Fig. 1(b)]. For the $\text{H}^-/\text{Cu}(100)$ system, in contrast, since the surface potential lacks sufficient surface-localizing reflectivity (it fails to support a surface state within the band gap), the states, confined parallelly by the ion, decay rapidly into the metal valence band, as indicated by the broad bump in the valence band of Cu(100) [Fig. 1(b)]. Therefore, these new resonances near Cu(111) are parallelly confined hybrids.

The surface state is not bound in the parallel direction. A resonance state that energetically lies above the surface state while being confined parallelly has to be less bound in the normal direction than the surface state. A reduction of the normal binding can be achieved by sliding up the potential at the bulk-vacuum interface, that is, by moving the mean position of the wave function in normal direction towards the ion. This increases the overlap between the ionic wave function and that of the confined state. Consequently, for a given ion-surface separation, we expect the lowest parallelly confined state to be populated first because of its strongest wave function overlap with the ion. This is seen in Fig. 2, which depicts the

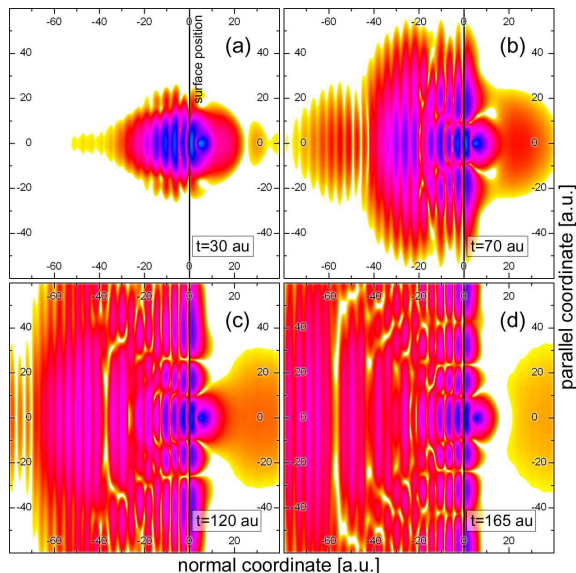


FIG. 2: (Color online) Wave packet densities (logarithmic scale) at $t = 30, 70, 120,$ and 165 a.u. for propagation at a fixed ion-surface separation of 5 a.u. The surface position is indicated by a vertical line.

propagated wave packet probability density $|\Phi(t)|^2$ at $t = 30, 70, 120$ and 165 a.u. for fixed $D = 5$ a.u. Figure 2(a) ($t = 30$ a.u.) shows an approximately nodeless structure outside the surface plane implying that over a short propagation time the ion populates predominantly the lowest parallelly confined state. However, at later times and increasing population of higher parallelly confined states, the wave packet spreads along the parallel co-ordinate forming additional nodal structures. Notably, since the parallel component of the wave packet outside the surface is a time-dependent linear combination of parallelly confined stationary states with *different* nodal structures, the position of a node moves with time. The ripples seen along the normal direction inside the bulk are due to the periodic bulk potential and a faint blob beyond $z \approx 20$ a.u. on the vacuum side [Fig. 2(b-d)] represents the evolution of weakly populated image states.

Fig. 3 shows the energy and the width of various resonances as a function of D . Our results for affinity level and surface state resonances are qualitatively similar to previous calculations[8]. At large distances, the energy [Fig. 3(a)] of the affinity level resonance (filled circles) is solely governed by image interactions leading to a good agreement with corresponding jellium results (opaque circles). In Fig. 3(b) on the other hand, affinity level resonance widths for Cu(111) are smaller than the jellium predictions at large distances, since in the jellium case no band gap exists and electrons can decay in the normal direction. The strong interaction, seen in the distance-dependent widths and energies between the affinity level resonance and the surface state resonance (filled squares) for small D , is the consequence of an indirect coupling between the corresponding discrete quasi-stationary states

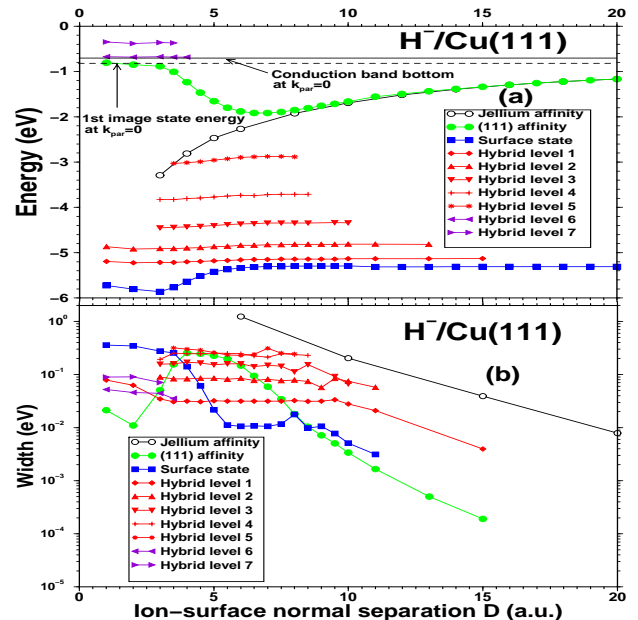


FIG. 3: (Color online) Energies and widths of various resonances as a function of the ion-surface distance.

through the surface state continuum[8]. Interestingly, both energy and width of the parallelly confined resonances depend only weakly on D (Fig. 3). We explain this near-stabilization by couplings of a given parallelly confined state with both affinity and surface state that have comparable strength. These couplings result in opposite level shifts and comparable rates (widths) for transitions between the affinity and parallelly confined state and between the parallelly confined state and the surface state. The same argument explains the stabilization of resonances just above the ionic resonance for very close D where the states are interacting with the ion and the conduction band. Furthermore, as discussed before, the state with maximum binding in the parallel direction has the strongest overlap with the affinity level and the weakest with the surface state. As a result, while it is “fed” by the ion the most, it decays through the surface state continuum the least acquiring a narrow width [Fig. 3(b)]. The counter-argument explains the large widths for minimally confined states in the parallel direction.

During the approach to the surface the projectile gradually decelerates in the normal direction along its incoming trajectory, owing to the repulsive interaction between its neutral core and surface atoms, until its normal velocity becomes zero at the point of closest approach. For specular reflection, it re-gains its original normal velocity. For a given initial kinetic energy and angle of incidence, we simulate the classical ion-trajectory by modeling the core-surface interaction via a plane-averaged interatomic potential[14]. This defines a distance of closest approach as a function of the initial normal velocity. Since the ion moves slowly near the surface, the adiabatic (fixed-ion) results (Figs. 1-3) provide a good guideline to understand the calculations for a moving ion. In Fig. 4, we present

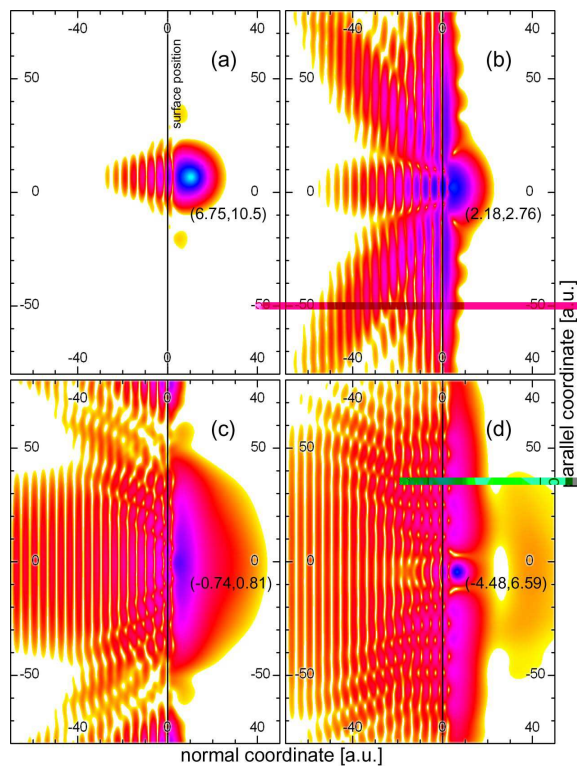


FIG. 4: (Color online) Wave packet densities (logarithmic scale) at times -320 a.u.(a), -110 a.u.(b), 20 a.u.(c), and 180 a.u.(d), relative to the time at which the point of closest approach is reached. The ion approaches the surface at an angle of 60° with respect to the surface and with an energy of 50 eV. Positions (X, D) are given in parenthesis, with X being relative to the point of closest approach.

four wave packet probability densities, a pair each from the incoming and the outgoing part of the trajectory of H^- ions with 50 eV asymptotic energy at 60° incidence with respect to the surface. In Fig. 4(a), $D = 10.5$ a.u., the ion predominantly populates the state confined most strongly in the parallel direction. Reaching $D = 2.76$ a.u., Fig. 4(b), the wave packet spreads over all available parallelly confined states, and clear nodal structures emerge symmetrically along the parallel direction outside the surface with each “bead” emanating a jet into the bulk. Electrons in the central jet have small parallel velocity indicating their ejection from the most tightly confined state. A steady increase of the parallel velocity is evidenced going symmetrically away from the center in parallel direction since the more distant jets originate from less strongly confined states. In Fig. 4(c), the ion arrives roughly at the distance of closest approach, 0.5 a.u., where the adiabatic energy position of the ionic resonance moves very close to the conduction band [Fig. 3(a)] and induces new resonances above the ionic level. Again, the node formation and resulting jets are seen, although the shape of the wave packet density is now dominated by a strong decay into the conduction band as well as by the subsequent population of image states, degenerate with the conduction band, on the vacuum side of the projec-

tile. A remarkable signature of the parallel confinement is finally seen on the outward excursion of the ion in Fig. 4(d) at $D = 6.59$ a.u.: the entrapment of the electron back in parallelly confined states results in decay-jets into the bulk and subsequent re-ionization of the projectile (note the strong trapping at the ion position). As an observable consequence of the strong participation of parallelly confined states in the decay near Cu(111), we find about 6% ion survival after the scattering of H^- from this surface as opposed to about 2% from Cu(100), which is free from this effect. A detailed comparative study will be published elsewhere[15].

In conclusion, we demonstrate significant parallel confinement effects in resonant neutralization of H^- near Cu(111) by directly analyzing the evolution of the active electron’s wave packet probability density. A surface-induced breakdown of the ionic spherical symmetry and significant reflectivity of the surface potential is responsible for this confinement. Finally, there is nothing special about Cu(111). Any of the surfaces, namely, Ag(111), Au(111), Pd(111) etc., supporting a surface state in the L -band gap is expected to show similar parallel confinement phenomena during the RCT process.

This work is supported by the NSF (grant PHY-0071035) and the Division of Chemical Sciences, Office of Basic Energy Sciences, Office of Energy Research, US DoE.

-
- [1] J.P. Gauyacq et al., in *Formation/Destruction of Negative Ions in Heavy Particle-Surface Collisions*, edited by V. Esaulov (Negative Ions, Cambridge University Press, 1996).
 - [2] H. Shao et al., in *Low Energy Ion-Surface Interactions*, edited by J.W. Rabalais (Wiley, New York, 1994) p. 118; J.J.C. Geerlings and J. Los, Phys. Rep. **190**, 133 (1990).
 - [3] B. Bahrim et al., Surf. Sci. **431** 193 (1999).
 - [4] P. Nordlander, Phys. Rev. B **46**, 2584 (1992).
 - [5] B. Bahrim and U. Thumm, Surf. Sci. **521** 84 (2002); P. Kürpick and U. Thumm, Phys. Rev. A **58**, 2174 (1998).
 - [6] F. Martin and M.F. Politis, Surf. Sci. **356**, 247 (1996).
 - [7] A.G. Borisov et al., Phys. Rev. Lett. **80**, 1996 (1998).
 - [8] A.G. Borisov et al., Phys. Rev. B **59**, 10935 (1999).
 - [9] W.H. Press et al., *Numerical Recipes in FORTRAN* (Cambridge University Press, Cambridge, 1993).
 - [10] U. Thumm, in *Book of Invited Papers, XXII International Conference on Photonic, Electronic, and Atomic Collisions, Santa Fe, NM*, edited by S. Datz et al. (Rinton Press, 2002) p. 592.
 - [11] L. Guillemot and V.A. Esaulov, Phys. Rev. Lett. **82**, 4552 (1999).
 - [12] J.S. Cohen and G. Fiorentini, Phys. Rev. A **33**, 1590 (1986).
 - [13] E.V. Chulkov et al., Surf. Sci. **437**, 330 (1999).
 - [14] J.P. Biersack and J.F. Ziegler, Nucl. Instrum. Meth. **194**, 93 (1982); J. Ducrée et al., Phys. Rev. A **60**, 3029 (1999).
 - [15] H.S. Chakraborty, T. Niederhausen, and U. Thumm, to be published.